9-30-2019

High Throughput Screening of 3D Printable Resins: Adjusting the Surface and Catalytic Properties of Multifunctional Architectures

J. Sebastián Manzano
Iowa State University and Ames Laboratory

Hsin Wang
Iowa State University and Ames Laboratory

Igor I. Slowing
Iowa State University and Ames Laboratory, islowing@iastate.edu

High Throughput Screening of 3D Printable Resins: Adjusting the Surface and Catalytic Properties of Multifunctional Architectures

Abstract

Identification of 3D printable materials is crucial to expand the breadth of physical and chemical properties attainable by additive manufacturing. Stereolithography (SLA), a widespread 3D printing method based on resin photo-polymerization, is ideally suited for exploring a large variety of monomers to produce functional three-dimensional solids of diverse properties. However, for most of the commercially available SLA 3D printers, screening monomers and resin compositions requires large volumes (~150 mL) in each printing cycle, making the process costly and inefficient. Herein, a high throughput block (HTB) adaptor was developed to screen arrays of monomers and resin compositions, consuming lower volumes (< 2 mL) and less time per print (< 1/16 based on a 4?4 matrix) than using the original hardware. Using this approach, a library of materials with different surface hydrophobicities were 3D printed by including long chain acrylates in the resins. In addition, several metal salts were dissolved in an acrylic acid-based resin, 3D printed and screened as heterogeneous catalysts for the selective aerobic oxidation of benzyl alcohol to benzaldehyde. Cu(II)-based resins produced the most active structures. Combinations of Cu(II) and long chain acrylate monomers were then used to 3D print complex catalytic architectures with varying degrees of hydrophobicity. Linear relationships were observed between 3D printed surface area, surface hydrophobicity and catalyst performance. For a high surface Schwarz P topology ca. 60 % enhancement in the catalytic activity of Cu(II) was attained by replacing the parent resin with one containing hydrophobic isodecyl groups, indicating that the immediate environment of the catalytic site affected its performance. The HTB enables fast screening of resins for 3D printing multifunctional architectures with intrinsic catalytic activity, tunable surface properties, and minimal waste.

Keywords

3D printing, stereolithography, high throughput, surface hydrophobicity, heterogeneous catalysis

Disciplines

Polymer and Organic Materials | Polymer Chemistry

High Throughput Screening of 3D Printable Resins: Adjusting the Surface and Catalytic Properties of Multifunctional Architectures

*J. Sebastián Manzano[1,2], Hsin Wang[1,2], Igor I. Slowing[1,2]**

[1]U.S. Department of Energy, Ames Laboratory, Ames, IA 50011-3020, USA

[2]Department of Chemistry, Iowa State University, Ames, IA 50011-3111, USA

*Corresponding author E-mail: islowing@iastate.edu

ABSTRACT

Identification of 3D printable materials is crucial to expand the breadth of physical and chemical properties attainable by additive manufacturing. Stereolithography (SLA), a widespread 3D printing method based on resin photo-polymerization, is ideally suited for exploring a large variety of monomers to produce functional three-dimensional solids of diverse properties. However, for most commercial SLA printers, screening monomers and resin compositions requires large volumes (~150 mL) in each printing cycle, making the process costly and inefficient. Herein, a high throughput block (HTB) adaptor was developed to screen arrays of monomers and resin compositions, consuming lower volumes (< 2 mL) and less time per print (< 1/16 based on a 4×4 matrix) than using the original hardware. Using this approach, a library of materials with different surface hydrophobicities were 3D printed by including long chain acrylates in the resins. In addition, several metal salts were dissolved in an acrylic acid-based resin, 3D printed and screened as benzyl alcohol oxidation catalysts. Cu(II)-based resins produced the most active structures. Combinations of Cu(II) and long chain acrylate monomers were then used to 3D print complex catalytic architectures with varying degrees of hydrophobicity. Linear relationships were observed between 3D printed surface area, surface hydrophobicity and catalyst performance. For a high surface Schwarz P topology ca. 60 %

enhancement in the catalytic activity of Cu(II) was attained by replacing the parent resin with one containing hydrophobic isodecyl groups, indicating that the immediate environment of the catalytic site affected its performance. The HTB enables fast screening of resins for 3D printing multifunctional architectures with intrinsic catalytic activity, tunable surface properties, and minimal waste.

KEYWORDS: 3D printing, stereolithography, high-throughput, surface hydrophobicity, heterogeneous catalysis

INTRODUCTION

3D printing is a novel technology to manufacture custom objects with intricate architectures directly from computer-based designs. In many cases these three-dimensional structures are too difficult to produce with traditional methods. The ability to 3D print materials with suitable properties has led to several applications in diverse fields like tissue engineering,[1-4] electronics,[5] ceramics,[6-9] mechanical devices,[10-16] pharmaceuticals,[17-20] periodic microstructures,[6,21] and catalysis.[22-25] Further development of these advanced applications requires controlling the physical and chemical properties of the objects produced. 3D printing methods based on photo-polymerization like stereolithography (SLA) yield higher resolution structures in a shorter time than other techniques, and hence are among the preferred approaches for additive manufacturing.[26,27] Because these methods are based on site-selective polymerization of

photo-active monomers, they can include molecular diversity either by variation in monomer structure (*i.e.* changes in carbon backbone, inclusion of additional functional groups) or by combination of different monomers (*i.e.* co-polymerization).[22,27-43] This diversity may hold the key to adjusting physical and chemical properties of multifunctional 3D printed architectures.

Nonetheless, developing resin compositions that produce three-dimensional structures with target chemical and physical characteristics can be expensive and time-consuming. These limitations are due to the conventional hardware setup of most SLA printers, which are commonly designed to use a single batch of resin per printing cycle in a relatively large volume tank (typically 150 mL). Inspired by a recent success in screening resins for inkjet printing,[40] we aimed to develop a direct screening approach for SLA 3D printing. Here, we introduce a high throughput screening approach consisting of compartmentalizing the build platforms and resin tanks of commercial SLA printers. This methodology allowed identification of active resin compositions by directly 3D printing functional structures. It also enabled production of a library of 3D printed materials with a wide spectrum of surface hydrophilicities/hydrophobicities and a library of 3D printed metal acrylates. The metal acrylate library was then screened to identify 3D printed structures that were catalytically active in the selective conversion of benzyl alcohol to benzaldehyde. More complex compositions were obtained by combining the

hydrophobic resins with the metal-containing resins to 3D print multifunctional architectures that displayed even higher activity for the same reaction.

EXPERIMENTAL

Materials.

Acetonitrile, cerium trinitrate hexahydrate, chromium trinitrate nonahydrate, cobalt dinitrate hexahydrate, copper diacetate monohydrate, iron tri(acetylacetonate), palladium dinitrate, gold trichloride trihydrate, erbium trinitrate pentahydrate, iridium trichloride, zinc dinitrate hexahydrate, allylamine, butyl, isobutyl, hexyl, 2 -ethylhexyl, isodecyl, octadecyl, and lauryl acrylates, acrylic acid, bis(2,4,6-trimethylbenzoyl)-phenylphosphine oxide (BAPO), tetramethyl-1-piperidinyloxy (TEMPO), poly(ethylene glycol) diacrylate (PEGDA), benzyl alcohol, propionitrile, and butyronitrile were acquired at Sigma-Aldrich. Antimony trichloride, nickel dinitrate hexahydrate, magnesium diiodide, bismuth trinitrate pentahydrate and cobalt dinitrate were bought at Fischer Scientific. All reagents were used without further purification.

Fused Filament Fabrication (FFF).

Computer aided designs were produced with OnShape (Cambridge, MA, USA) and converted into STL format. The resin tanks and platform matrices were manufactured using polypropylene filament in a Makerbot Replicator 2x^{TM} (New York City, NY, USA). The size of the resin tanks in the 4×4 matrix was 25×25×6 mm each.

Polydimethylsiloxane (PDMS) layer.

To help the peeling process during printing, a layer of PDMS was applied to the bottom of the compartmentalized tanks. Following the manufacturer recommended ratios, 40 g of 10:1 ratio of the Sylgard® 184 two-part solution was prepared and 2 mL from this mixture were added to each tank. The tanks containing PDMS were cured for 24 h in an oven at 50 ºC. The cured PDMS-covered tanks were then ready for use as reservoirs for the resins.

Parent resin preparation.

The parent resin consisting of acrylic acid and PEGDA was prepared as reported before.[22]

Hydrophobic resins.

The parent resin was mixed with each acrylate in varying ratios according to Table S1. For allylamine the mixture (allylamine: acrylic acid mole ratio 0.13) was prepared in an ice bath to prevent heat evolution and avoid pre-polymerization. The combinations were thoroughly mixed in a homogenizer (14 000 rpm, 5 min), and poured into the low volume resin tanks adapted to a FormLabs Form 1+™ 3D printer (Somerville, MA, USA).

Metal containing resins.

5 mL of the parent resin was mixed with 0.11 mmol of the respective metal salt and sonicated until complete dissolution of the metal salts (Table S2). The solutions were poured into the low volume resin tanks adapted to the FormLabs Form 1+™ 3D printer.

Surface functionalization of 3D printed objects.

A 3D printed cube was added to a methylene chloride solution of N,N′-Dicyclohexylcarbodiimide (48 mM, 5 mL) in a 20 mL vial and set in an orbital shaker (1 h, 300 rpm). 0.15 mmol of the respective amine (i.e. oleylamine, isopropyl amine or *tert*-butylamine) were then added and the vial was shaken for 16 h more. The printed cubes were then thoroughly washed with methylene chloride and dried before measuring the water contact angle.

SLA 3D printing.

Computer aided designs were produced with OnShape (Cambridge, MA, USA), converted into STL format, and printed in the FormLabs Form 1+™ 3D printer. The settings used for non-metal containing resins were: *laser power*: 62 mW, *first layer passes*: 10, *other layer passes*: 2, and *early layer passes*: 2. For metal-containing resins the parameters were: *laser power*: 62 mW, *first layer passes*: 10, *other layer passes*: 5, and *early layer passes*: 5. The residual non-polymerized resin was extracted from the 3D printed solids by soaking in acetone for 5 min. The solids were then cured in a Rayonet photo-reactor (λ = 320 nm, 20 min).

Oxidation of benzyl alcohol.

A 3D printed metal-polymer composite hollow cube was introduced into a 5 mL vial containing a solution of benzyl alcohol (20 µL, 0.19 mmol) and Tetramethyl-1-piperidinyloxy radical (TEMPO, 12 mg, 76 µmol) in acetonitrile (1 mL). The vial was then

crimped with a silicon/aluminum cap, added a stir bar and the solution was stirred at 100 °C and 200 rpm for 6 h. A 10 µL aliquot was diluted in ethanol (1 mL) and analyzed by GC-MS (Agilent 7890A, 5975C, HP-5MS column). The program initiated at 60 °C, a temperature ramp of 5 °C $min^{-1}$was applied until reaching 150 °C. This was followed by a second ramp of 20 °C min^{-1} until 280 °C, after which the temperature was held constant for 10 min. The reactions were run in parallel using an aluminum heating block reactor. Catalytic activity screening was based on the relative intensities of benzaldehyde (ca. 5.15 min retention time) to benzyl alcohol (ca. 5.95 min retention time) peaks, and selection criteria were established as <5%, 5-10% and >10% corresponding to low, moderate and high catalytic activity. Decane was used as internal standard for calculating actual conversion values (as opposed to screening experiments). To evaluate the effect of solvent polarity on reactivity acetonitrile was replaced with propionitrile or butyronitrile.

Contact angle measurements.

The water contact angles were measured using a Ramé-Hart 200 (p/n 200-U1) goniometer. The 3D printed cubes were mounted on the sample holder, followed by addition of a ca. 2 µL drop of deionized water. Images were acquired using a SuperSpeed USB 3.0 CCD camera and the slope of the tangent to the drop at the water-solid interface was analyzed using Image J software.

RESULTS AND DISCUSSION

First, we designed a high throughput block (HTB) adaptor set consisting of a 4×4 matrix of build platforms that could be attached to the z-stage of a Formlabs 1+™ 3D printer, and a fitting matrix of 4×4 low volume (2 mL) resin tanks (**Figure 1a, b)**. This configuration was chosen to maximize the number of resin tanks for the dimensions of the 3D printer. However, the dimensions and distribution of the tanks and platforms can be adapted to any target size and configuration (Figure S1). The adaptors were then produced by fused filament fabrication (FFF) using a polypropylene (PP) filament in a Makerbot Replicator 2x™ 3D printer. The 4×4 matrix resin tanks were designed to be 25×25×6 mm each. To facilitate peeling of the printed layers, the resin tanks were coated and cured with a 3 mm polydimethylsiloxane (PDMS) layer (Sylgard® 184 silicone elastomer) as a pre-printing process. To prevent leakage during the cruing of PDMS the 4×4 resin tanks matrix was fixed onto a Z-vat resin tank using hot melt adhesive (Ad Tech™). Aluminum plates were added to the build platforms to ensure adhesion of the 3D printed objects (**Figure 1c**).

Using the custom 4×4 HTB we 3D printed a library of 32 materials from resins containing the parent mixture (acrylic acid, BAPO and PEGDA) and acrylate esters of varying chain lengths and branching, or allylamine. The mole ratios of acrylate esters or allylamine to acrylic acid were varied from 0.05 to 0.7 (**Table S1**). The resins were 3D printed as hollow cubes (7 mm sides, **Figure S2)** so that material hydrophobicity could be assessed by measuring water contact angles on their flat surfaces (**Figure S3-S11**).

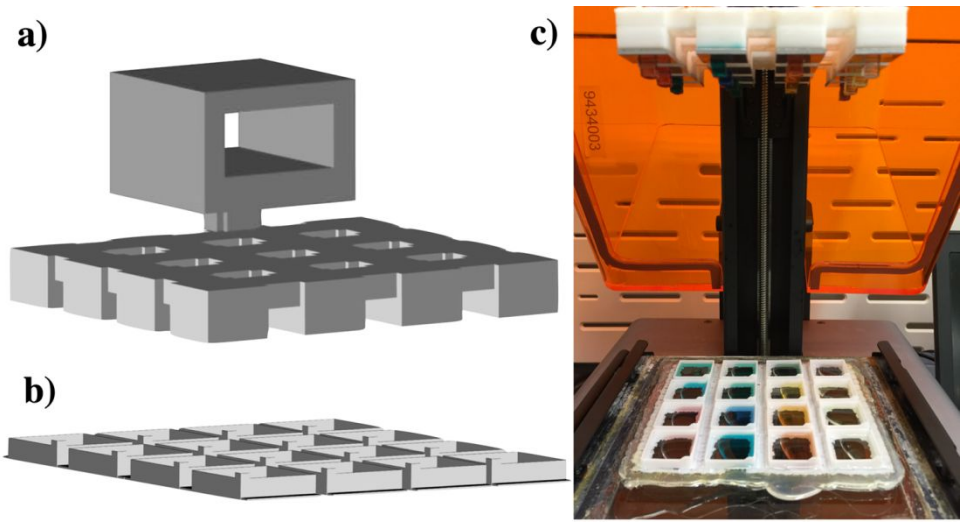

Figure 1. STL design of a) build platform, b) resin tanks and c) complete 4×4 set up for high throughput block (HTB) adaptor.

The parent resin, containing only acrylic acid and PEGDA, had a water contact angle of 42°, characteristic of a hydrophilic surface. The hydrophilic character is likely due to the carboxylic acid moieties on the surface of the 3D printed polymer.[22] Incorporation of linear acrylate esters in the C_4 to C_{12} range resulted in a more hydrophobic surface with a moderate increase in the water contact angle to about 65° at ca. 0.1 acrylate ester : acrylic acid (AE : AA) molar ratios (Figure 2a). The larger contact angle indicates that the hydrocarbon chains of the esters may be exposed on the surface of the objects. A larger increase to about 80° was observed when using the C_{18} ester at 0.1 AE : AA molar ratio. The larger effect of C_{18} suggests that in addition to being exposed on the surface, its long hydrocarbon chain may be covering some of the hydrophilic surface carboxylates.

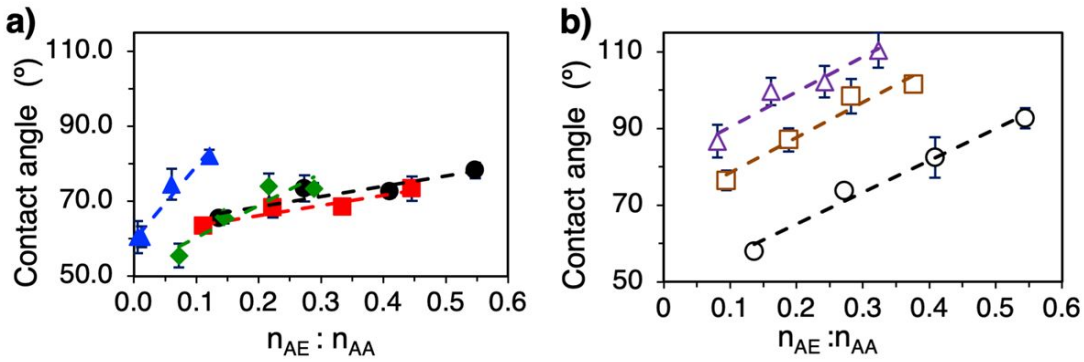

Figure 2. Changes in water contact angle with the amount of acrylate esters (AE) relative to acrylic acid (AA) used in the resin for a) linear (black circles = butyl, red diamonds = hexyl, green squares= lauryl, blue triangles = octadecyl) and b) branched AE (black circles = isobutyl, brown squares = 2-ethylhexyl, purple triangles = isodecyl). Error bars correspond to the standard deviations of two measurements.

The water contact angles of the 3D printed materials displayed a linear dependence on the amount of ester in the monomer mixture, indicating that the surface density of the hydrophobic moieties is proportional to their concentration in the resin. While the rate of increase in contact angle with AE : AA molar ratio was very similar for C_4 and C_6, it was about 3 and 7 times larger for C_{12} and C_{18} respectively. It must be noted that the longer chain esters had a lower solubility in the resin which limited the amount that could be effectively incorporated into the 3D printed objects. Analysis of the water contact angles of the cubes 3D printed with branched AE monomers indicated a more dramatic effect on surface hydrophobicity: isobutyl acrylate, 2-ethylhexyl acrylate and isodecyl acrylate reached maximum contact angles of 93°, 102° and 110° respectively (**Figure 2b**).

In contrast to the enhanced hydrophobicity produced by alkyl acrylate monomers, the use of allylamine as a co-polymer led to 3D printed objects with higher hydrophilicity than that obtained with the parent resin. For example a resin with allylamine : AA molar ratio 0.13 gave a solid with a water contact angle of 17° (**Figure 3**). The enhanced hydrophilicity is likely due to proton transfer between the amine and the carboxylic acid groups resulting in a zwitterionic surface.[44]

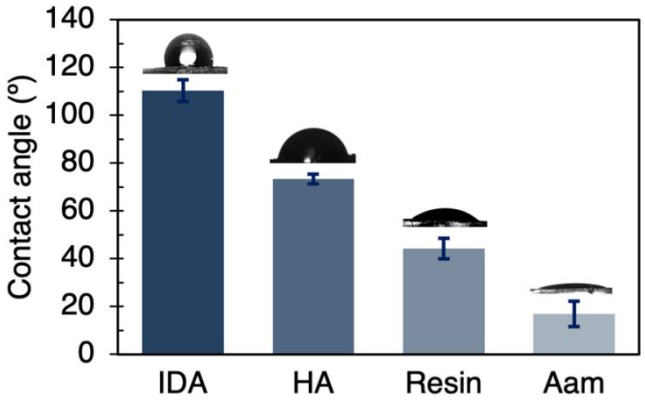

Figure 3. Variations in the wettability of 3D printed resins as a function of the co-monomer included in its composition (mole fractions of co-monomers relative to acrylic acid: isodecyl acrylate (IDA) 0.32, hexyl acrylate (HA) 0.45, allylamine (Aam) 0.13. Error bars correspond to the standard deviations of two measurements.

An additional way to modify the surface hydrophobicity of 3D printed AA resins is by reacting the pendant carboxylic acids with alcohols or amines. We evaluated this post-printing method using carbodiimide to activate surface carboxyls for coupling with isopropyl, tert-butyl and oleyl amines. Bond formation was confirmed by the emergence

of the characteristic amide bands (1630 cm^{-1} and 1550 cm^{-1}) in the infrarred spectra of the 3D printed structures (**Figure 4**). Even though the same amounts of amine (0.15 mmol) were added to each of the 3D printed cubes, FTIR showed large differences between them. While the cubes modified with small amines (tert-butyl- and isopropyl-amine) had more intense 1550 cm^{-1} (amide II) than 1720 cm^{-1} (AA and PEGDA carbonyl) bands, the cubes modified with oleylamine had a much more intense 1720 cm^{-1} than 1550 cm^{-1} band. In spite of their lower ratio of amide to carboxyl/ester signal, the oleylamine-modified cubes produced a significantly larger water contact angle (123°) than those modified with isopropylamine and tert-butylamine (90° and 73°, respectively). Importantly, this post-printing modification approach can be combined with the co-polymerization method to produce multifunctional three dimensional objects.

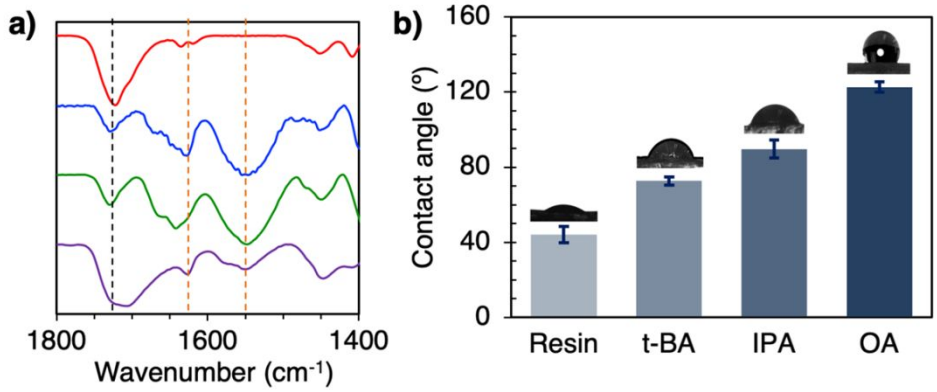

Figure 4. a) Attenuated total reflectance infrared spectra of 3D printed structures before (red) and after grafting with tert-butylamine (blue), isopropylamine (green) and oleylamine (purple). Discontinuous lines correspond to PEGDA and AA carbonyl (black), and amide I and II (orange) bands. b) Water contact angles of 3D printed surfaces

modified with non-polar groups. t-BA = t-butylamine, IPA = isopropylamine, OA = oleylamine. Error bars correspond to the standard deviations of two measurements.

We have recently demonstrated that 3D printing by SLA can produce architectures with intrinsic catalytic activity. Here, we used the HTB adaptor to evaluate 16 metal salts as potential precursors for 3D printed catalysts. First, we dissolved the salts (0.11 mmol) in a resin consisting of PEGDA and AA (5 mL resin, 11.6 and 204 mmol respectively). The resins were then 3D printed to form hollow top- and bottom-less cubes (4 faces, 8×8 mm sides with 0.5 mm thick walls, Figure S12). This simple topology allowed rapid printing that in turn facilitated quick adjustments of the parameters to the metals' properties. For example, because the metal salts had some absorbance at the laser wavelength (405 nm, Figure S13) they required a larger number of laser passes to polymerize in an effective and controlled fashion (5 passes at 62 mW laser power compared to only 2 passes for the normal resin). The 0.5 mm walls still provided a large surface to volume ratio (4.25 : 1) to expose the metal catalyst and enable rapid screening for activity. A large surface to volume ratio is especially relevant because the polymeric matrix has low porosity and a penetration depth limited to ca. 70 μm.[22] The products were designated as M-HC, where M represents the metal used. Interestingly, heating the 3D printed Ag-HC and Au-HC at 40 ˚C for 1h, led to a change from colorless to brown and purple, respectively. The development of color can be ascribed to nanoparticle formation, as previously shown by Fantino et al.[31,45,46] and Chibac et al.[47] No changes in appearance were observed for the

remaining M-HC upon heating at 40 °C. Absence of signals in the XRD of the 3D printed solids between 10 and 90 $2\theta°$ further suggested lack of crystalline particles formation.

The M-HC were then screened as catalysts for the conversion of benzyl alcohol into benzaldehyde. The selective oxidation of primary alcohols to aldehydes is relevant because of the ubiquity of these functionalities in active principles of several pharmaceuticals, fragrances, dyes, and agrochemicals.[48,49] Traditionally, these reactions require stoichiometric amounts of toxic, expensive and corrosive oxidizing agents like DMSO/acyl chloride combinations,[50] hypervalent iodine,[30,51] or heavy metals.[52] Consequently, supported transition metal ions have been investigated as potential catalysts for this transformation with the aim of conducting a greener process.[53] To screen for potential catalytic activity the M-HC were added to a mixture of benzyl alcohol (20 µL, 0.38 mmol) and TEMPO (12 mg, 0.076 mmol) in acetonitrile (1 mL), sealed with a silicone septum, and heated to 100 °C for 6 h in a parallel reaction block (200 rpm). The reaction mixtures were then analyzed by GC-MS. Comparison of the relative intensities of benzaldehyde to benzyl alcohol peaks indicated some activity for Bi, Co, Er, Ir, Mg and Sb (5-10% relative intensity), moderate for Ce, Cr, Ni and Zn (10-15%), and significantly higher for Cu (25%) (Table S2). The remaining M-HC, as well as a HC with no metal salt embedded, did not show any catalytic activity under these reaction conditions. Considering Cu-HC produced the highest benzaldehyde levels in the screening, we used this metal for further catalyst 3D printing studies. While some copper species have already

been reported as active for this reaction,[54-62] there are no previous reports of the selective oxidation of alcohols to aldehydes using Zn or Er salts co-catalyzed by TEMPO.

We then explored how the topology of 3D printed Cu-based catalysts determined the amount of surface area exposed and thereby affected conversion. Importantly, because the 3D printed polymers are not porous,[26] their surface areas were not measured by nitrogen physisorption (typical BET surface areas lower than 1 m^2 g^{-1}) but estimated based on macroscale topology. Therefore, we 3D printed a series of triply periodic minimal surface (TPMS) constructs. These surfaces consist of two interpenetrating meandering paths that lack self-intersections and fill up space in a continuous fashion.[63-66] The 3D printed TPMS structures were: Chmutov octic, diamond-1, diamond-3, gyroid, Schoen-I-6, Schoen-manta and Schwarz P (**Figure 5**).[67] To include a low surface structure we also 3D printed a hypercube model. While these intricate catalyst-containing geometries are too difficult to manufacture by conventional methods, 3D printing allows fast and easy production, and even modifications to each of them at any desired scale. The 3D surfaces were designed and scaled to an 8×8×8 mm cubic volume that fit a test tube leaving space for a magnetic stir bar (**Figure S14**). The benzyl alcohol oxidation reactions were performed for 21 h at 100 °C and revealed differences in conversion between the 3D printed catalyst architectures. Plotting conversion versus the surface area of the structures (calculated with 3Dtool software™) indicated that all the structures had the same intrinsic activity, and the differences in performance were mainly due to the amount of surface

provided by the specific topology (**Figure 6a**). This result demonstrates that 3D printing can be employed to improve chemical conversions by translating optimized surface packings into active three dimensional catalysts.

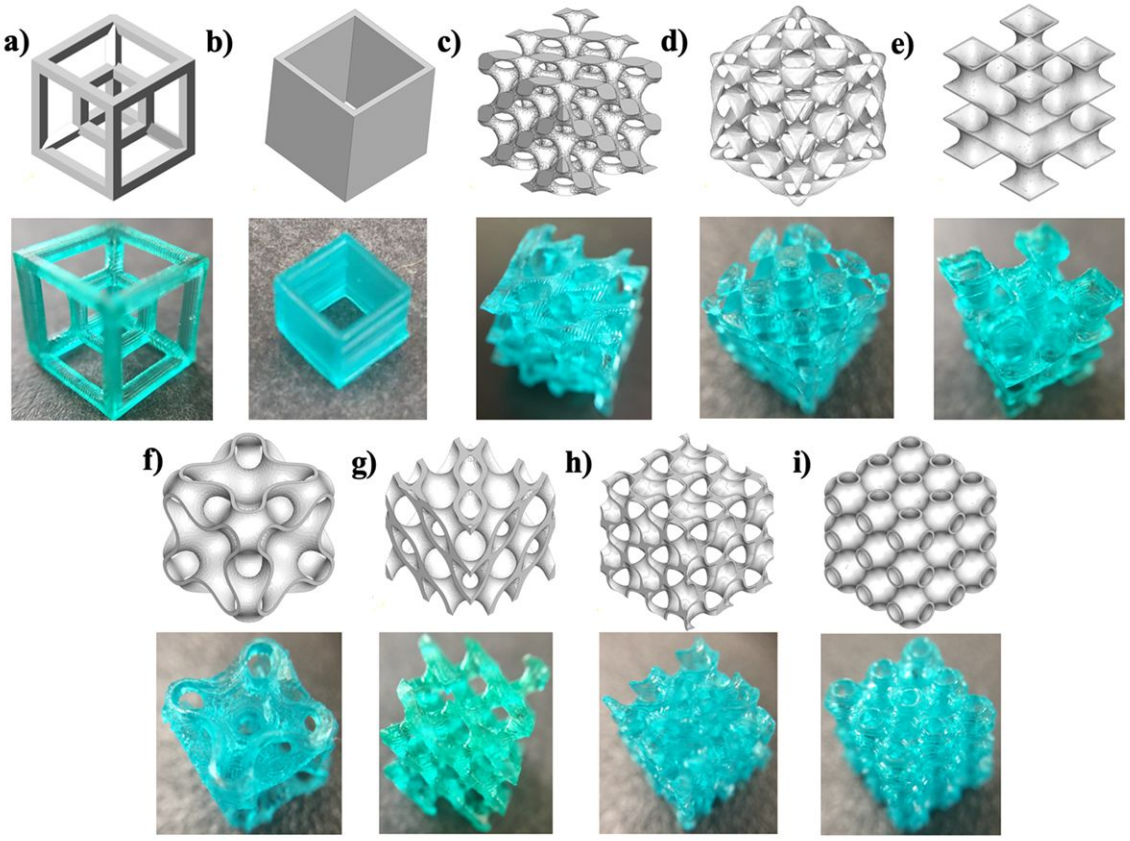

Figure 5. STL designs of complex geometries and the corresponding 3D printed Cu-containing catalysts: a) Hyper cube, b) hollow cube, c) diamond-1, d) Chmutov Octic, e), Schoen-I-6, f) Schoen-manta, g) diamond-3, h) Gyroid, and i) Schwarz P (primitive), minimal surfaces. All cubes are designed to have 8 mm sides.

Because low polarity environments can increase conversion in the aerobic oxidation of alcohols catalyzed by metals,[68-70] we tested the performance of the most active 3D printed

geometry (Cu-Schwarz P) in three solvents of different polarities (acetonitrile: ε = 37.5, propionitrile: ε = 27.7, and butyronitrile: ε = 20.7). Our results confirmed an inverse relationship between the solvents' dielectric constants and benzyl alcohol conversion (**Figure 6b**). This dependence of conversion on polarity suggested that the performance of Cu-Schwarz P topology could be improved by increasing the hydrophobicity of the 3D printed material using the approaches described before. Therefore, we 3D printed a series of Cu-Schwarz P structures using resins that included different acrylate esters with varying hydrophobicities. In addition to the unmodified resin (contact angle 44°) we used resins with ester modifiers having the following $n_{modifier}$: n_{resin} ratios: of 0.14 for butyl acrylate, 0.30 for 2-ethylhexyl acrylate and 0.33 for isodecyl acrylate. These modified resins gave contact angles of ca. 65°, 100°, and 110°, respectively. Using the modified Cu-Schwarz P-materials as catalysts for the benzyl alcohol oxidation in acetonitrile resulted in a linear dependence of conversion on their water contact angles (**Figure 6c**). The resulting trend is consistent with the one observed using solvents of varying dielectric constants, i.e. higher hydrophobicity leads to improved oxidation activity, with the isodecyl-Cu-Schwarz P being ca. 60 % more active than the parent Cu-Schwarz P catalyst. These results demonstrate that the immediate environment of the catalytic Cu sites in the materials 3D printed with acrylate esters was dominated by the components of the original resin rather than the reaction solvent, and prove that catalytic performance can be improved both by adjusting surface topology and chemical composition of the 3D printed catalysts.

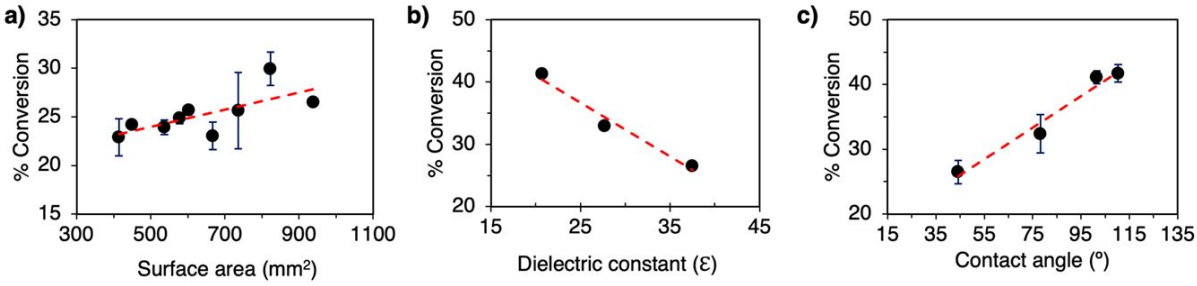

Figure 6. a) Dependence of the apparent catalytic activity of 3D printed Cu-containing complex geometries on their surface areas. Catalytic activity of b) 3D printed Cu-Schwarz P topologies in solvents with increasing polarity (acetonitrile, propionitrile, butyronitrile), and c) 3D printed Cu-Schwarz P topologies prepared from resins with varying hydrophobicities (solvent: acetonitrile). Reaction conditions: 2 mL solvent, 0.15 mmol TEMPO, and 0.76 mmol benzyl alcohol stirred at 100 °C for 21 h. Error bars are the standard deviations of three catalytic conversions.

CONCLUSIONS

This work presents a method to increase the throughput of commercial SLA 3D printers and enable screening of functional 3D printable resins. The high-throughput block (HTB) adaptors consisting of arrays of miniaturized build platforms and resin tanks can be custom designed and 3D printed to suit the needs of any target application. The approach proved useful for producing a series of 3D printed materials with varying surface hydrophobicities and allowed establishing structure-property relationships between the

molecular structure of monomers and the hydrophobicity of solids. While the hydrocarbon chain length of the acrylate esters increased the hydrophobicity of the 3D printed surfaces, chain branching resulted in a much larger effect. The HTB were also used to produce a series of 3D printed metal-containing polymers that were screened as potential catalysts in the selective oxidative conversion of benzyl alcohol to benzaldheyde, leading to the discovery of new TEMPO co-catalysts with moderate (Ce, Cr, Ni, Zn), and mild activity (Bi, Co, Er, Ir, Mg, Sb). In addition, we used the HTB to 3D print a series of Cu-containing complex structures and demonstrated the dependence of catalytic conversion on the amount of surface that can be efficiently packed in a given volume. The Shwarz P topology gave the best catalytic activity, consistent with its highest surface area. Finally, because the catalytic activity of Cu in the reaction of benzyl alcohol to benzaldehyde increases with decreasing solvent polarity, we modified the surface chemistry of Cu-Schwarz P with acrylic esters and demonstrated that the activity increased with the materials' surface hydrophobicity, the largest activity enhancement being ca. 60 % using an isodecyl acrylate-containing resin. This result suggests that the surface properties of 3D printed catalysts can ultimately determine the performance of the active sites, and that this approach is capable of directly producing multifunctional materials with tunable structure and composition.

ASSOCIATED CONTENT

Supporting Information

The Supporting Information is available free of charge at the ACS Publications website.

Pictures of different HTB setups and water contact angle measurements, additional tables, UV-Vis spectra, and Stl files of the HTB and catalytic structures.

CONFLICTS OF INTEREST

There are no conflicts to declare.

ACKNOWLEDGEMENTS

This research is supported by the U.S. Department of Energy, Office of Basic Energy Sciences, Division of Chemical Sciences, Geosciences, and Biosciences, through the Ames Laboratory Catalysis Science program. The Ames Laboratory is operated for the U.S. Department of Energy by Iowa State University under Contract No. DE-AC02-07CH11358

REFERENCES

(1) Barry, R. A.; Shepherd, R. F.; Hanson, J. N.; Nuzzo, R. G.; Wiltzius, P.; Lewis, J. A. Direct-Write Assembly of 3D Hydrogel Scaffolds for Guided Cell Growth. *Adv. Mater.* **2009**, *21*, 2407-2410.

(2) Boland, T.; Xu, T.; Damon, B.; Cui, X. Application of Inkjet Printing to Tissue Engineering. *Biotechnol. J.* **2006**, *1*, 910-917.

(3) Mohanty, S.; Larsen, L. B.; Trifol, J.; Szabo, P.; Burri, H. V. R.; Canali, C.; Dufva, M.; Emnéus, J.; Wolff, A. Fabrication of Scalable and Structured Tissue Engineering Scaffolds using Water Dissolvable Sacrificial 3D Printed Moulds. *Mater. Sci. Eng. C* **2015**, *55*, 569-578.

(4) Habibovic, P.; Gbureck, U.; Doillon, C. J.; Bassett, D. C.; van Blitterswijk, C. A.; Barralet, J. E. Osteoconduction and Osteoinduction of Low-Temperature 3D Printed Bioceramic Implants. *Biomater.* **2008**, *29*, 944-953.

(5) Ahn, B. Y.; Duoss, E. B.; Motala, M. J.; Guo, X.; Park, S.-I.; Xiong, Y.; Yoon, J.; Nuzzo, R. G.; Rogers, J. A.; Lewis, J. A. Omnidirectional Printing of Flexible, Stretchable, and Spanning Silver Microelectrodes. *Science* **2009**, *323*, 1590-1593.

(6) Smay, J. E.; Gratson, G. M.; Shepherd, R. F.; Cesarano, J.; Lewis, J. A. Directed Colloidal Assembly of 3D Periodic Structures. *Adv. Mater.* **2002**, *14*, 1279-1283.

(7) Tubío, C. R.; Azuaje, J.; Escalante, L.; Coelho, A.; Guitián, F.; Sotelo, E.; Gil, A. 3D Printing of a Heterogeneous Copper-Based Catalyst. *J. Catal.* **2016**, *334*, 110-115.

(8) Tubío, C. R.; Guitián, F.; Gil, A. Fabrication of ZnO Periodic Structures by 3D Printing. *J. Eur. Ceram. Soc.* **2016**, *36*, 3409-3415.

(9) Lewis, J. A. Direct Ink Writing of 3D Functional Materials. *Adv. Funct. Mater.* **2006**, *16*, 2193-2204.

(10) Au, A. K.; Huynh, W.; Horowitz, L. F.; Folch, A. 3D-Printed Microfluidics. *Angew. Chem., Int. Ed.* **2016**, *55*, 3862-3881.

(11) Ho, C. M. B.; Ng, S. H.; Li, K. H. H.; Yoon, Y.-J. 3D Printed Microfluidics for Biological Applications. *Lab Chip* **2015**, *15*, 3627-3637.

(12) Waheed, S.; Cabot, J. M.; Macdonald, N. P.; Lewis, T.; Guijt, R. M.; Paull, B.; Breadmore, M. C. 3D Printed Microfluidic Devices: Enablers and Barriers. *Lab Chip* **2016**, *16*, 1993-2013.

(13) Kitson, P. J.; Rosnes, M. H.; Sans, V.; Dragone, V.; Cronin, L. Configurable 3D-Printed Millifluidic and Microfluidic 'Lab on a Chip' Reactionware Devices. *Lab Chip* **2012**, *12*, 3267-3271.

(14) Choong, Y. Y. C.; Maleksaeedi, S.; Eng, H.; Wei, J.; Su, P.-C. 4D Printing of High Performance Shape Memory Polymer using Stereolithography. *Mater. Design* **2017**, *126*, 219-225.

(15) Wu, H.; Chen, P.; Yan, C.; Cai, C.; Shi, Y. Four-dimensional Printing of a Novel Acrylate-based Shape Memory Polymer using Digital Light Processing. *Mater. Design* **2019**, *171*, 107704.

(16) Zhao, T.; Yu, R.; Li, X.; Cheng, B.; Zhang, Y.; Yang, X.; Zhao, X.; Zhao, Y.; Huang, W. 4D Printing of Shape Memory Polyurethane via Stereolithography. *Eur. Polym. J.* **2018**, *101*, 120-126.

(17) Gross, B. C.; Erkal, J. L.; Lockwood, S. Y.; Chen, C.; Spence, D. M. Evaluation of 3D Printing and Its Potential Impact on Biotechnology and the Chemical Sciences. *Anal. Chem.* **2014**, *86*, 3240-3253.

(18) Goyanes, A.; Wang, J.; Buanz, A.; Martínez-Pacheco, R.; Telford, R.; Gaisford, S.; Basit, A. W. 3D Printing of Medicines: Engineering Novel Oral Devices with Unique Design and Drug Release Characteristics. *Molec. Pharm.* **2015**, *12*, 4077-4084.

(19) Melchels, F. P. W.; Feijen, J.; Grijpma, D. W. A Review on Stereolithography and its Applications in Biomedical Engineering. *Biomater.* **2010**, *31*, 6121-6130.

(20) Goole, J.; Amighi, K. 3D Printing in Pharmaceutics: A New Tool for Designing Customized Drug Delivery Systems. *Int. J. Pharm.* **2016**, *499*, 376-394.

(21) Compton, B. G.; Lewis, J. A. 3D-Printing of Lightweight Cellular Composites. *Adv. Mater.* **2014**, *26*, 5930-5935.

(22) Manzano, J. S.; Weinstein, Z. B.; Sadow, A. D.; Slowing, I. I. Direct 3D Printing of Catalytically Active Structures. *ACS Catal.* **2017**, *7*, 7567-7577.

(23) Díaz-Marta, A. S.; Tubío, C. R.; Carbajales, C.; Fernández, C.; Escalante, L.; Sotelo, E.; Guitián, F.; Barrio, V. L.; Gil, A.; Coelho, A. Three-Dimensional Printing in Catalysis: Combining 3D Heterogeneous Copper and Palladium Catalysts for Multicatalytic Multicomponent Reactions. *ACS Catal.* **2018**, *8*, 392-404.

(24) Konarova, M.; Aslam, W.; Ge, L.; Ma, Q.; Tang, F.; Rudolph, V.; Beltramini, J. N. Enabling Process Intensification by 3 D Printing of Catalytic Structures. *ChemCatChem* **2017**, *9*, 4132-4138.

(25) Zhou, X.; Liu, C.-j. C. Three-dimensional Printing for Catalytic Applications: Current Status and Perspectives. *Adv. Funct. Mater.* **2017**, *27*, 1701134.

(26) Bartolo, P., ed. *Stereolithography Materials, Processes and Applications*; Springer, New York, NY, U.S.A. **2011**, 340.

(27) Ligon, S. C.; Liska, R.; Stampfl, J.; Gurr, M.; Mülhaupt, R. Polymers for 3D Printing and Customized Additive Manufacturing. *Chem. Rev.* **2017**, *117*, 10212-10290.

(28) Yu, R.; Yang, X.; Zhang, Y.; Zhao, X.; Wu, X.; Zhao, T.; Zhao, Y.; Huang, W. Three-Dimensional Printing of Shape Memory Composites with Epoxy-Acrylate Hybrid Photopolymer. *ACS Appl. Mater. Interfaces* **2017**, *9*, 1820-1829.

(29) Valentin, T. M.; Leggett, S. E.; Chen, P.-Y.; Sodhi, J. K.; Stephens, L. H.; McClintock, H. D.; Sim, J. Y.; Wong, I. Y. Stereolithographic Printing of Ionically-Crosslinked

Alginate Hydrogels for Degradable Biomaterials and Microfluidics. *Lab Chip* **2017**, *17*, 3474-3488.

(30) Uyanik, M.; Ishihara, K. Hypervalent Iodine-Mediated Oxidation of Alcohols. *Chem. Commun.* **2009**, 2086-2099.

(31) Taormina, G.; Sciancalepore, C.; Bondioli, F.; Messori, M. Special Resins for Stereolithography: In Situ Generation of Silver Nanoparticles. *Polymers* **2018**, *10*, 212.

(32) Kumar, S.; Hofmann, M.; Steinmann, B.; Foster, E. J.; Weder, C. Reinforcement of Stereolithographic Resins for Rapid Prototyping with Cellulose Nanocrystals. *ACS Appl. Mater. Interfaces* **2012**, *4*, 5399-5407.

(33) Palaganas, N. B.; Mangadlao, J. D.; de Leon, A. C. C.; Palaganas, J. O.; Pangilinan, K. D.; Lee, Y. J.; Advincula, R. C. 3D Printing of Photocurable Cellulose Nanocrystal Composite for Fabrication of Complex Architectures via Stereolithography. *ACS Appl. Mater. Interfaces* **2017**, *9*, 34314-34324.

(34) Sutton, J. T.; Rajan, K.; Harper, D. P.; Chmely, S. C. Lignin-Containing Photoactive Resins for 3D Printing by Stereolithography. *ACS Appl. Mater. Interfaces* **2018**, *10*, 36456-36463.

(35) Sinh, L. H.; Harri, K.; Marjo, L.; Minna, M.; Luong, N. D.; Jürgen, W.; Torsten, W.; Matthias, S.; Jukka, S. Novel Photo-Curable Polyurethane Resin for Stereolithography. *RSC Adv.* **2016**, *6*, 50706-50709.

(36) Ni, R.; Qian, B.; Liu, C.; Liu, X.; Qiu, J. A Cross-Linking Strategy with Moderated Pre-Polymerization of Resin for Stereolithography. *RSC Adv.* **2018**, *8*, 29583-29588.

(37) Seo, H.; Heo, S. G.; Lee, H.; Yoon, H. Preparation of PEG Materials for Constructing Complex Structures by Stereolithographic 3D Printing. *RSC Adv.* **2017**, *7*, 28684-28688.

(38) Zhang, J.; Xiao, P. 3D Printing of Photopolymers. *Polymer Chem.* **2018**, *9*, 1530-1540.

(39) Wallin, T. J.; Pikul, J. H.; Bodkhe, S.; Peele, B. N.; Mac Murray, B. C.; Therriault, D.; McEnerney, B. W.; Dillon, R. P.; Giannelis, E. P.; Shepherd, R. F. Click Chemistry Stereolithography for Soft Robots that Self-Heal. *J. Mater. Chem. B* **2017**, *5*, 6249-6255.

(40) Louzao, I.; Koch, B.; Taresco, V.; Ruiz-Cantu, L.; Irvine, D. J.; Roberts, C. J.; Tuck, C.; Alexander, C.; Hague, R.; Wildman, R.; Alexander, M. R. Identification of Novel "Inks" for 3D Printing Using High-Throughput Screening: Bioresorbable Photocurable Polymers for Controlled Drug Delivery. *ACS Appl. Mater. Interfaces* **2018**, 6841-6848.

(41) Ge, Q.; Sakhaei, A. H.; Lee, H.; Dunn, C. K.; Fang, N. X.; Dunn, M. L. Multimaterial 4D Printing with Tailorable Shape Memory Polymers. *Sci. Rep.* **2016**, *6*, 31110.

(42) Choi, J.-W.; Kim, H.-C.; Wicker, R. Multi-Material Stereolithography. *J. Mater. Proc. Technol.* **2011**, *211*, 318-328.

(43) Voet, V. S. D.; Strating, T.; Schnelting, G. H. M.; Dijkstra, P.; Tietema, M.; Xu, J.; Woortman, A. J. J.; Loos, K.; Jager, J.; Folkersma, R. Biobased Acrylate Photocurable Resin Formulation for Stereolithography 3D Printing. *ACS Omega* **2018**, *3*, 1403-1408.

(44) Beck, A. J.; Whittle, J. D.; Bullett, N. A.; Eves, P.; Mac Neil, S.; McArthur, S. L.; Shard, A. G. Plasma Co-Polymerisation of Two Strongly Interacting Monomers: Acrylic Acid and Allylamine. *Plasma Proc. Polym.* **2005**, *2*, 641-649.

(45) Fantino, E.; Chiappone, A.; Calignano, F.; Fontana, M.; Pirri, F.; Roppolo, I. In Situ Thermal Generation of Silver Nanoparticles in 3D Printed Polymeric Structures. *Mater.* **2016**, *9*, 589-.

(46) Sciancalepore, C.; Moroni, F.; Messori, M.; Bondioli, F. Acrylate-Based Silver Nanocomposite by Simultaneous Polymerization–Reduction Approach via 3D Stereolithography. *Composites Commun.* **2017**, *6*, 11-16.

(47) Chibac, A. L.; Melinte, V.; Buruiana, T.; Mangalagiu, I.; Buruiana, E. C. Preparation of Photocrosslinked Sol-Gel Composites Based on Urethane-Acrylic Matrix, Silsesquioxane Sequences, TiO_2, and Ag/Au Nanoparticles for use in Photocatalytic Applications. *J. Polym. Sci. A - Polym. Chem.* **2015**, *53*, 1189-1204.

(48) Ciriminna, R.; Ghahremani, M.; Karimi, B.; Pagliaro, M. Electrochemical Alcohol Oxidation Mediated by TEMPO-like Nitroxyl Radicals. *Chem. Open* **2017**, *6*, 5-10.

(49) Yu, Y.; Lu, B.; Wang, X.; Zhao, J.; Wang, X.; Cai, Q. Highly Selective Oxidation of Benzyl Alcohol to Benzaldehyde with Hydrogen Peroxide by Biphasic Catalysis. *Chem. Eng. J.* **2010**, *162*, 738-742.

(50) Steinhoff, B. A.; Fix, S. R.; Stahl, S. S. Mechanistic Study of Alcohol Oxidation by the Pd(OAc)2/O2/DMSO Catalyst System and Implications for the Development of Improved Aerobic Oxidation Catalysts. *J. Am. Chem. Soc.* **2002**, *124*, 766-767.

(51) Richardson, R. D.; Wirth, T. Hypervalent Iodine Goes Catalytic. *Angew. Chem., Int. Ed.* **2006**, *45*, 4402-4404.

(52) Ming-Lin, G.; Hui-Zhen, L. Selective Oxidation of Benzyl Alcohol to Benzaldehyde with Hydrogen Peroxide over Tetra-Alkylpyridinium Octamolybdate Catalysts. *Green Chem.* **2007**, *9*, 421-423.

(53) Sheldon, R. A. Recent Advances in Green Catalytic Oxidations of Alcohols in Aqueous Media. *Catal. Today* **2015**, *247*, 4-13.

(54) Zhang, X.; Dong, W.; Luan, Y.; Yang, M.; Tan, L.; Guo, Y.; Gao, H.; Tang, Y.; Dang, R.; Li, J.; Wang, G. Highly Efficient Sulfonated-Polystyrene–Cu(II)@$Cu_3(BTC)_2$ Core–Shell Microsphere Catalysts for Base-Free Aerobic Oxidation of Alcohols. *J. Mater. Chem. A* **2015**, *3*, 4266-4273.

(55) Guan, M.; Wang, C.; Zhang, J.; Zhao, Y. Practical Organic Solvent-Free $Cu(OAc)_2$/DMAP/TEMPO-Catalyzed Aldehyde and Imine Formation from Alcohols under Air Atmosphere. *RSC Adv.* **2014**, *4*, 48777-48782.

(56) Zhang, G. F.; Han, X. W.; Luan, Y. X.; Wang, Y.; Wen, X.; Xu, L.; Ding, C. R.; Gao, J. R. Copper-Catalyzed Aerobic Alcohol Oxidation under Air in Neat Water by using a Water-Soluble Ligand. *RSC Adv.* **2013**, *3*, 19255-19258.

(57) Taher, A.; Kim, D. W.; Lee, I.-M. Highly Efficient Metal Organic Framework (MOF)-Based Copper Catalysts for the Base-Free Aerobic Oxidation of Various Alcohols. *RSC Adv.* **2017**, *7*, 17806-17812.

(58) Kumpulainen, E. T. T.; Koskinen, A. M. P. Catalytic Activity Dependency on Catalyst Components in Aerobic Copper–TEMPO Oxidation. *Chem. Eur. J.* **2009**, *15*, 10901-10911.

(59) Gamez, P.; Arends, I. W. C. E.; Reedijk, J.; Sheldon, R. A. Copper(ii)-Catalysed Aerobic Oxidation of Primary Alcohols to Aldehydes. *Chem. Commun.* **2003**, 2414-2415.

(60) Figiel, P. J.; Sibaouih, A.; Ahmad, J. U.; Nieger, M.; Räisänen, M. T.; Leskelä, M.; Repo, T. Aerobic Oxidation of Benzylic Alcohols in Water by 2,2,6,6-Tetramethylpiperidine-1-oxyl (TEMPO)/Copper(II) 2-N-Arylpyrrolecarbaldimino Complexes. *Adv. Synth. Catal.* **2009**, *351*, 2625-2632.

(61) Wang, Q.; Zhang, Y.; Zheng, G.; Tian, Z.; Yang, G. Base-Free Copper-Catalyzed Aerobic Oxidation of Benzylic Alcohols with N-Benzylidene-N,N-Dimethylthane-1,2-Diamine and TEMPO. *Catal. Commun.* **2011**, *14*, 92-95.

(62) Salinas Uber, J.; Vogels, Y.; van den Helder, D.; Mutikainen, I.; Turpeinen, U.; Fu, W. T.; Roubeau, O.; Gamez, P.; Reedijk, J. Pyrazole-Based Ligands for the [Copper–TEMPO]-Mediated Oxidation of Benzyl Alcohol to Benzaldehyde and Structures of the Cu Coordination Compounds. *Eur. J. Inorg. Chem.* **2007**, *2007*, 4197-4206.

(63) Abueidda, D. W.; Bakir, M.; Abu Al-Rub, R. K.; Bergström, J. S.; Sobh, N. A.; Jasiuk, I. Mechanical Properties of 3D Printed Polymeric Cellular Materials with Triply Periodic Minimal Surface Architectures. *Mater. Design* **2017**, *122*, 255-267.

(64) Abueidda, D. W.; Abu Al-Rub, R. K.; Dalaq, A. S.; Lee, D.-W.; Khan, K. A.; Jasiuk, I. Effective Conductivities and Elastic Moduli of Novel Foams with Triply Periodic Minimal Surfaces. *Mech. Mater.* **2016**, *95*, 102-115.

(65) Travitzky, N.; Bonet, A.; Dermeik, B.; Fey, T.; Filbert-Demut, I.; Schlier, L.; Schlordt, T.; Greil, P. Additive Manufacturing of Ceramic-Based Materials. *Adv. Eng. Mater.* **2014**, *16*, 729-754.

(66) Thomas, N.; Sreedhar, N.; Al-Ketan, O.; Rowshan, R.; Abu Al-Rub, R. K.; Arafat, H. 3D Printed Triply Periodic Minimal Surfaces as Spacers for Enhanced Heat and Mass Transfer in Membrane Distillation. *Desalination* **2018**, *443*, 256-271.

(67) Lord, E. A.; Mackay, A. L. Periodic Minimal Surfaces of Cubic Symmetry. *Curr. Sci.* **2003**, *85*, 346-362.

(68) Singappuli-Arachchige, D.; Manzano, J. S.; Sherman, L. M.; Slowing, I. I. Polarity Control at Interfaces: Quantifying Pseudo-solvent Effects in Nano-Confined Systems. *ChemPhysChem* **2016**, *17*, 2982-2986.

(69) Chen, Y. X.; Qian, L. F.; Zhang, W.; Han, B. Efficient Aerobic Oxidative Synthesis of 2-Substituted Benzoxazoles, Benzothiazoles, and Benzimidazoles Catalyzed by 4-Methoxy-TEMPO. *Angew. Chem.* **2008**, *120*, 9470-9473.

(70) Shi, S.; Liu, M.; Zhao, L.; Wang, M.; Chen, C.; Gao, J.; Xu, J. Catalytic Oxidation of Alcohol to Carboxylic Acid with a Hydrophobic Cobalt Catalyst in Hydrocarbon Solvent. *Chem. Asian. J.* **2017**, *12*, 2404-2409.

Figure for the TOC